Engineering Structures 279 (2023) 115554

Contents lists available at ScienceDirect

Engineering Structures

journal homepage: www.elsevier.com/locate/engstruct

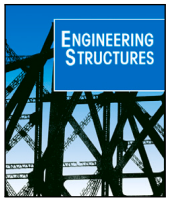

Exploring the potential of the critical shear crack theory for reinforced and post-tensioned glass beams: Initial analysis and experiments

Jagoda Cupać [a,b], Christian Louter [c,*], Alain Nussbaumer [a]

[a] Resilient Steel Structures Laboratory (RESSLab), École Polytechnique Fédérale de Lausanne (EPFL), GC B3 495, Station 18, 1015 Lausanne, Switzerland
[b] Institute of Building Construction, Technische Universität Dresden, August-Bebel-Strasse 30, 01219 Dresden, Germany
[c] Structural Design & Building Engineering, Faculty of Civil Engineering & Geosciences, Delft University of Technology, Stevinweg 1, 2628 CN Delft, The Netherlands

ARTICLE INFO

Keywords:
Reinforced and post-tensioned glass beam
Shear resistance
Post-fracture limit state
Critical shear crack
Shear-transfer actions
Double-notched mixed-mode test

ABSTRACT

In the evolution of structural glass beam elements, the requirements for post-fracture load bearing capacity and safe failure behaviour have led to the development of reinforced and post-tensioned beams. Maximum bending capacity in the post-fracture state is normally associated with extensive yielding of the reinforcement, providing a safe failure mechanism through apparent ductility of the composite beam section. This can be achieved as long as the propagation of primary flexural cracks does not compromise the transfer of shear from the load points to the supports. Although shear failure is typically not critical for the ultimate limit state design of 'normal' unreinforced glass beams, it may govern the load-bearing and deformation capacity in the post-fracture state for reinforced and post-tensioned glass beams. This paper presents exploratory experiments and initial analysis of the shear failure phenomenon in the post-fracture state of reinforced and post-tensioned glass beams. Potential shear transfer mechanisms are identified based on the critical shear crack theory developed for reinforced concrete members and applied in the analysis of shear failures observed in four-point bending tests of post-tensioned glass beams. The behaviour of fractured laminated glass under mixed-mode (tension+shear) loading is explored on a limited set of small-scale double-notched glass specimens, demonstrating the feasibility of the applied test methodology. Preliminary findings of the present study may serve as a basis for further investigations of shear resistance of glass beams. Typical shear failure kinematics and suitable constitutive laws of the applied materials need further investigation in order to provide design recommendations for the prediction of shear resistance of reinforced and post-tensioned glass beams.

1. Introduction

Glass design in construction follows the conventional ultimate (ULS) and serviceability limit state (SLS) requirements in order to ensure adequate material strength, stability and user comfort. Additionally, due to the possibility of brittle glass fracture, specific performance requirements need to be considered to ensure safe behaviour upon glass fracture. These requirements have recently been formulated as two additional limit states for future design codes: fracture limit state (FLS), which considers the structural behaviour during fracture, and post-fracture limit state (PFLS) [1].

In the design evolution of glass beam elements, the requirements for post-fracture load bearing capacity and safe failure behaviour have led to the development of reinforced and post-tensioned beams, which have been extensively investigated over the past few decades (see overview of experimental research in [2]). The addition of a reinforcing material (e.g. steel, timber, CFRP, GFRP) in the tensile zone of a glass element, similarly to reinforced concrete, provides a load bearing mechanism that can sustain significant loads upon glass fracture. Compressive pre-stress, additionally applied in a post-tensioned beam system, further increases the initial fracture resistance of glass in bending. Existing studies have explored a variety of beam compositions (monolithic and laminated glass with single or multiple tendons, mechanically anchored — incorporated in the glass section [3,4] or applied externally [5,6] — or adhesively bonded tendons pre-stressed by an external mechanism [7]) and loading conditions (simple and continuous beam, varying temperature, humidity and load duration). Bedon and Louter [8] have investigated analytical and numerical methods for prediction of load-bearing capacity and post-fracture behaviour of structural glass beams with embedded GFRP, CFRP or steel reinforcement rods. More recently, Silvestru et al. [9] applied adhesively bonded strips made of iron-based shape memory alloy for post-tensioning glass elements. Multiple failure modes leading to the ultimate failure in the post-fracture state have been investigated; the maximum post-fracture capacity has been

* Corresponding author.
E-mail address: Christian.Louter@tudelft.nl (C. Louter).

https://doi.org/10.1016/j.engstruct.2022.115554
Received 14 July 2022; Received in revised form 30 November 2022; Accepted 27 December 2022
Available online 11 January 2023

associated with the tensile failure of the tendon or the crushing of glass in compression after extensive yielding of the reinforcement, known as *the normal reinforced state* [10]. In this way, the reinforced glass beam reaches its full flexural capacity, while the yielding of the reinforcement ensures a safe near-ductile behaviour preceding the ultimate failure.

Full flexural capacity of reinforced or post-tensioned glass beams can be achieved as long as the propagation of primary flexural cracks does not compromise the transfer of shear from the load point to the supports. If the cracks propagate in the shear span along the theoretical direct compression strut, the strength of a member is limited with respect to its flexural capacity and the shear resistance may become decisive in the post-fracture state. There is currently no method for the calculation of shear resistance of glass beams implemented in structural design codes, while only a limited number of research studies have focused on this aspect of load-bearing behaviour of structural glass beams.

Louter et al. [11] tested 3.2 m long SentryGlas® (SG) laminated annealed glass beams, reinforced with a hollow square steel section, in four-point bending in a lateral buckling test setup. The beam shear slenderness, i.e. the ratio of the shear span to effective depth, was ~4. One out of three specimens was tested to full destruction; remaining tests were stopped at the displacement limit of the setup. The ultimate failure of the beam was caused by a distinctive shear crack, which slowly developed in the post-fracture state. The interlayer locally buckled along the densely fractured shear crack.

Agnetti and Speranzini [12] investigated hybrid steel-fibre reinforced beams consisting of a laminated annealed glass section of various cross-sectional properties and steel fibres adhesively bonded at the tensile glass edge. Although shear failure was not specifically reported, a critical shear crack can be seen in the published material, which shows a crack pattern of a PVB-laminated glass beam after a four-point bending test, with a shear slenderness of 3.5. The impact of the shear crack on the failure behaviour was not discussed.

In the study of simple and pre-stressed hybrid steel-glass beams by Firmo et al. [13], shear failure was reported in four-point bending tests of both simple and pre-stressed samples. The beams consisted of an SG-laminated annealed glass section (2 × 10 mm × 300 mm) and two steel flanges (100 mm × 10 mm) adhesively bonded at the top and bottom glass edge. Pre-stressed series additionally incorporated two external steel cables with an offset inducing a hogging bending moment. The beam shear slenderness in the four-point bending setup was ~3.2. The development of shear cracks in the post-fracture state caused a significant drop in the bending stiffness and post-fracture load capacity, leading to ultimate failure once the debonding of the lower flange propagated from the root of the shear crack towards the vertical support. In the pre-stressed series, additional asymmetry caused by the shear cracks led to diverging loads in the cables. The cable eccentricity resulted in glass crushing in the anchorage area.

Wang et al. [14] reported a distinctive shear failure mode observed in an experimental study of mechanical behaviour of composite glass beams under in-plane loads. The beam specimens with a length of 1.8 m were composed of a double layered fully-tempered PVB-laminated glass web (2 × 6 mm/10 mm) and two 5–10 mm thick steel flanges, bonded with a relatively flexible silicone adhesive to form an H or I section composite beam. All test beams were designed with a uniform aspect ratio (depth of the glass web/clear beam span) and shear slenderness, equal to 0.14 and 2.08 respectively. In four-point bending tests, the fully-tempered glass panes broke suddenly into small glass particles which formed a diagonal pattern extending from the support to the load point. The failure was initiated in the compression zone by local stress concentration under the load point which caused edge delamination in the glass laminate, resulting in a *shear compression* failure. The analytical model developed in the study focused on this distinctive local compressive failure mode.

Campione et al. [15] analysed experimentally and theoretically the flexural behaviour of hybrid glass beams with a rectangular cross-section, with a focus on moment-to-shear interaction. The beams were composed of three annealed glass layers bonded with an acrylic adhesive (3 × 6 mm × 200 mm) and reinforced with steel plates embedded in the glass laminate at the bottom of the glass beams (6 mm × 25/50 mm). The beams of 0.9, 1.3 and 1.7 m length were tested in three-point bending; the shear slenderness was 2, 3 and 4, respectively. All the beams developed flexural cracks at the initial fracture load and shear cracks reaching the ultimate peak load. The authors reported two modes of ultimate shear failure: *shear compression* for beams with shear slenderness of 2, and *diagonal tension/splitting* for higher shear slenderness of 4. An analytical model was developed for preliminary design of hybrid glass beams, which predicts the initial glass fracture, ultimate failure in flexure with yielding of steel plates and shear compression failure. The model is based on plane section theory in flexure and determines the load-bearing capacity of hybrid glass beams in flexure and shear as sum of contributions due to beam and arching actions. In the prediction of shear failure, the model is governed by the crushing of the glass, i.e. the failure of inclined compression strut carrying shear from the load point to the vertical support. Additional shear transfer mechanisms associated with higher shear slenderness, i.e. diagonal splitting mode, are not explicitly considered.

In a recent study by Zhang et al. [16], ultimate failure caused by *diagonal splitting* in the flexural-shear region was observed in four-point bending tests on aluminium reinforced glass beam specimens. Specimens with a length of 1.4 m were composed of two sheets of PVB laminated annealed glass (2 × 5/10 mm × 140 mm) and a 6061-T6 aluminium alloy bar (10 mm × 10/20 mm) bonded to the bottom glass edge. Three series of reinforced beams (with varying beam composition and lateral support conditions) were tested in four-point bending with a constant beam shear slenderness of 3. One out of three specimens in each series failed due to a critical shear crack which quickly propagated towards the loading point, resulting in the diagonal splitting in the flexural-shear region[1]. Flexural resistance and deformation capacity of these three specimens was significantly lower. Since the initiation point of the critical shear cracks appeared relatively far from the pure-bending area under maximum tensile stress, the authors attributed this failure mode to local stress concentrations caused by excessive use of stiff glue for the attachment of strain gauges along the glass edge. However, this could also be attributed to the random distribution of flaw sizes induced by grinding and the resulting scatter in the tensile strength of glass. Experimental results were compared to the existing analytical model for prediction of flexural resistance of reinforced glass beams, proposed by Louter et al. [11], and the above mentioned model by Campione et al. [15], which includes the prediction of shear resistance. Both models provided unsafe estimations, particularly with reference to the ultimate failure loads resulting from the diagonal splitting.

Therefore, this paper explores an alternative model based on the critical shear crack theory (CSCT). This theory is developed for reinforced concrete members without transverse reinforcement [17,18], and in the current paper its application is attempted for the analysis of reinforced and post-tensioned glass beams. A qualitative analysis of shear transfer in glass beams is based on the observations of flexural behaviour of 1.5 m long SG-laminated glass beams, shown in Fig. 1, reinforced and post-tensioned through stainless steel tendons. The beams were tested in four-point bending in a wider experimental study [7], where several specimens developed a distinctive critical shear crack (CSC). The shear crack led to sudden failure of the specimen, preceding the attainment of the full flexural capacity of the beam, which reduced its ultimate load-bearing capacity and post-fracture ductility. The observed failure mode corresponds with *diagonal splitting*, reported in previous research, which has a significant impact on the reduction of flexural resistance and ductility, while it cannot be effectively

[1] The remaining reinforced specimens failed due to crushing of the glass in compression, crack-induced debonding or lateral-torsional buckling.

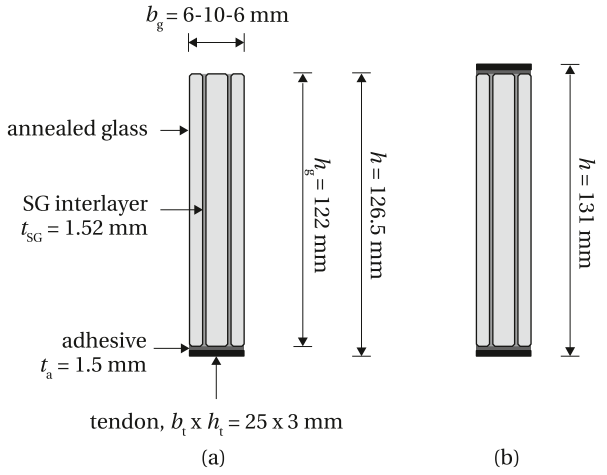

Fig. 1. Cross-sectional properties of glass beams post-tensioned through (a) single — series AS, or (b) double adhesively bonded tendon — series AMD [7].

predicted with existing analytical models. The application of the CSCT allows for the analysis of various shear transfer actions potentially activated through the kinematics of the diagonal shear crack, which may contribute to the shear strength of reinforced and post-tensioned beams in the post-fracture state. As such, it can contribute to better understanding of the mechanisms of shear transfer in glass beams and provide a basis for the development of a suitable prediction model for a safe design of reinforced and post-tensioned glass beams.

The critical shear crack theory is first introduced in Section 2, followed by the analysis of crack kinematics of a beam specimen that failed in shear in Section 3. Since the test measurements did not focus on the development of the CSC as it appeared unexpectedly, this initial qualitative analysis is based on a sequence of images that captured the development of the shear cracks during four-point bending tests. Additionally, the paper investigates the feasibility of a testing methodology for the simulation of stresses at the interface of a CSC subjected to opening (tension) and sliding (shear). The results of a limited set of exploratory experiments on small-scale pre-cracked SG-laminated glass specimens under mixed-mode loading is presented in Section 4. The future prospects of research on shear resistance of glass beams are discussed in Section 5, with the conclusions of the present study given in Section 6.

2. Critical shear crack theory

According to the CSCT, a shear failure can occur in glass beam elements due to the propagation of primary flexural cracks along the theoretical compression strut carrying shear directly from the load point to the support. The formation of a critical shear crack limits the strength of a member with respect to its flexural capacity, as the strength of the inclined compression strut is reduced by the presence of the crack. A failure in shear may happen before yielding of the tendon, governing the strength and ductility of the beam, or after yielding, when increasing rotations at the plastic plateau increase the width of the cracks, limiting the strength of various shear-carrying mechanisms. In the latter case, the shear failure governs the ductility, without affecting the maximum load capacity [19]. Since glass beams cannot be strengthened through additional transversal reinforcement, as concrete structures, without a detrimental effect on transparency, understanding of the mechanism of shear failure is particularly important. Specific shear transfer mechanisms in glass are here identified in analogy with the concrete behaviour described by the CSCT, supported by the observations from the four-point bending tests on post-tensioned glass beams, with an invariable shear span of 4.

After cracking induced by bending, shear can be transferred through various actions, depending on the location, shape and kinematics of the cracks. Concrete theory differentiates between *the arching action*, i.e. an inclined compression strut carrying shear from the load point to the vertical support, assuming a constant force in the tensile reinforcement/tendon (Fig. 2(a–b)), and *beam shear-transfer actions*, which keep a constant lever arm between the tension and compression chord, while the force in the tendon varies according to the bending moment distribution (Fig. 2(c–f)) [20]. The following *shear-transfer actions* may potentially contribute to the shear strength of reinforced and post-tensioned glass beams in the post-fracture state:

- *Cantilever action* - inclined struts and ties develop between two flexural cracks, acting as a cantilever beam fixed in the compression zone. The shear is transferred by the inclination of the compression chord, until the crack, developing with an inclination towards the load point, opens and interrupts the tension tie of the cantilever;
- *Residual tensile strength of glass* - for low crack openings, a certain level of tensile stresses may be transferred near the crack tip. This capacity diminishes with increasing crack opening (softening);
- *Surface interlock* - similarly to aggregate interlock in concrete, the roughness of the crack surface due to crack undulations, changes in direction, and overlapping of multiple crack branches, can generate shear and compressive stresses, depending on the opening (w) and relative slip (δ) between the lips of the crack;
- *Crack-bridging by the interlayer(s)* - accompanying surface interlock, in laminated glass beams, the interlayer is activated through shear action with the uncracked glass surfaces surrounding the crack, providing a bridge between the crack lips. Due to the opening and relative slip of the crack lips, the interlayer is subjected to tensile and shear stresses (mixed mode). The amount of shear transfer that can be sustained depends on the bond behaviour at the glass-interlayer interface, in relation with the crack slip and opening, and the tensile and shear capacity of the interlayer material;
- *Dowelling action* - the shear is transferred through the tendon, which acts as a dowel between the lips of the crack. The tendon is activated (in shear and bending) through the adhesive bond, which is subjected to tensile stresses induced by the relative vertical displacement of the crack lips.

The governing shear-transfer mechanism depends on the shear slenderness of the beam, i.e. the ratio of the shear span, a_s, to effective depth, d, which can be described by the *Kani's valley* (Fig. 3). For small slenderness, $a_s/d < \gamma_1$, the arching action is the governing mechanism; the cracks practically do not develop through the inclined compression strut, allowing the beam to reach the flexural strength, $Q_R = Q_{flex}$. For larger slenderness, $\gamma_1 < a_s/d < \gamma_2$, the cracks can partly penetrate the strut, decreasing the shear strength of a member ($Q_R < Q_{flex}$); the compression strut deviates to avoid the cracks, developing an elbow-shaped form. The failure is characterised by a stable propagation of cracks [21]. For slenderness values $a_s/d > \gamma_2$, the ratio between the shear strength and flexural strength starts to increase with the activation of various beam shear-transfer actions. Typically, a critical shear crack develops, leading to a sudden failure. For very large slenderness values, $a_s/d > \gamma_3$, the flexural strength is reached before the critical shear crack can develop and compromise the maximum post-fracture capacity [20].

The application of post-tensioning enhances the shear resistance of a beam by limiting the opening of the cracks. In reference to the Kani's valley, the effect of the compressive pre-load P can be interpreted as a reduction of the beam slenderness, a_s/d, schematically shown in Fig. 4, which compares the position of the theoretical compression strut in a reinforced beam without (a) and with the application of post-tensioning (b). It can be seen that, due to the application of the pre-load, no cracks can develop near the vertical support, which may postpone the

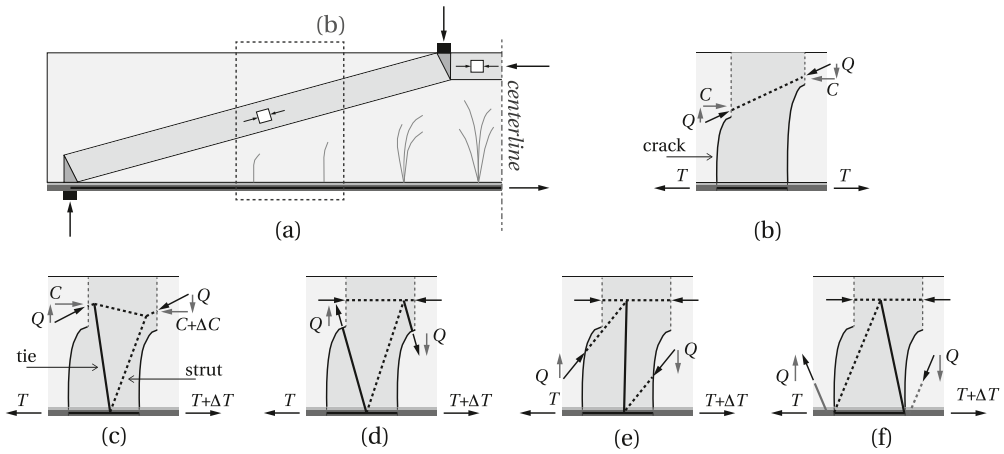

Fig. 2. Shear-transfer mechanisms, adapted from [20] for reinforced and post-tensioned glass beams: (a-b) arching action; (c) cantilever action; (d) residual tensile strength of glass; (e) surface interlock, crack-bridging by the interlayer(s); (f) dowelling action; C — compression; T — tension; Q — shear.

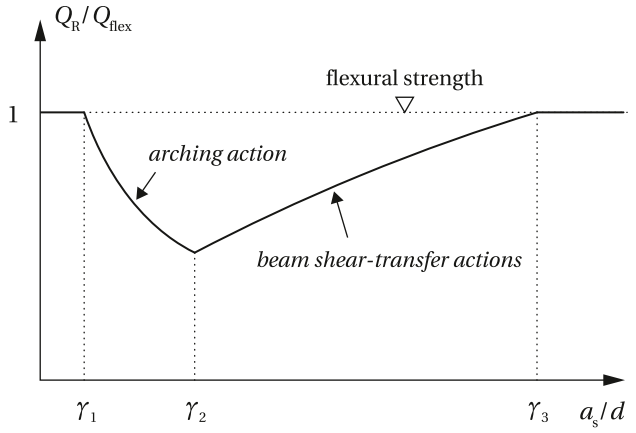

Fig. 3. Kani's valley, adapted from [20]: governing shear-transfer mechanism depending on the beam slenderness.

shear failure of the beam [21]. The effective (mechanical) shear span $a_{eff} = a_s - 2Pz/Q$, where P is the applied post-tensioning load, Q is the vertical load = reaction at the support, and z is the lever arm of the internal forces induced by bending in the post-fracture state.

3. Analysis of crack kinematics

Reinforced and post-tensioned SG-laminated glass beams with flat stainless steel tendons were investigated in a wider experimental study by the authors which focused on flexural behaviour of post-tensioned beams [7]. The study included three beam systems: (1) AS — glass beams post-tensioned through adhesively bonded single tendon placed along the bottom glass edge (Fig. 1(a)); (2) AMD — glass beams with adhesively bonded, mechanically post-tensioned double tendon placed along the top and bottom glass edge (Fig. 1(b)); and (3) MD — mechanically post-tensioned glass beams with double tendon placed along the top and bottom glass edge without an adhesive connection[2]. Structural behaviour of the beams was explored in four-point bending tests on 1.5 m long specimens, with a support span of 1400 mm, load span of 400 mm and a shear span of 500 mm. The beams were vertically simply supported on cylindrical steel rollers, one fixed and one free for longitudinal displacement. Lateral supports were placed at 200 mm from the vertical supports (AS), or integrated in the vertical supports (AMD). The tests were performed at ambient indoor conditions at an initial displacement rate of 1 mm/min, which was subsequently increased to 2 mm/min and 5 mm/min in the post-fracture state to shorten the duration of the test. A more detailed description of the beam specimens, the post-tensioning methods and the test setup can be found in [7], together with the results of the complete experimental study.

The post-tensioned beam specimens that exhibited distinctive shear failure in the four-point bending tests are shown in Fig. 5, in their final state following ultimate failure. The specimen label indicates the series (AS, AMD; Fig. 1), the level of applied pre-load in kN (PT25/50) and the specimen number in the referenced series. Specimens AS-PT25#2 and AS-PT25#3 (Fig. 5(a), 5(b)) failed at 95% and 78% of the predicted maximum flexural resistance,[3] respectively, with 70%–80% lower deformation capacity, while the specimen AMD-PT50#1 in Fig. 5(c) reached its maximum flexural capacity. This is illustrated in Fig. 6, which shows the load–displacement graphs of the complete series AS and AMD, with the specimens that developed a CSC highlighted in red. The failure quickly followed the formation of the CSC, resulting in debonding of the tendon. Significant crack propagation triggered by the sudden failure in shear resulted in the dense cracking pattern visible in the images.

The mechanical fixing of the tendon, applied at the beam ends of the specimen AMD-PT50#1 during post-tensioning and four-point bending, stabilised the final stage of the ultimate failure,[4] allowing a closer analysis of the CSC kinematics, presented in Fig. 7. As a result of rather low fracture toughness of glass, initial cracking induced by bending is generally accompanied by a high energy release, resulting in multiple crack branching, visible in Fig. 7(a) for the three primary flexural cracks as they appeared in the left shear span. As the leftmost crack propagated in shear, it turned from the tips of the branches towards the load introduction point, forming a slightly sloped crack, with an angle of ~ 20° (7(b), 7(c)). The overlapping crack paths originating from the multiple crack branches (in multiple glass layers) generated a certain degree of surface roughness along the crack lips. A centre of

[2] Series MD is not further discussed in this paper since the tested specimens generally failed due to lateral torsional buckling, before any shear cracks could be observed.

[3] Compared to the average failure load of the remaining specimens in the series that failed due to steel rupture.

[4] After the failure of the bond between the tendon and the glass, shear force was transferred to the bolt connecting the tendon to the steel anchor at the beam end, causing a rupture of the tendon at the bolt hole. The yielding at the bolt hole temporarily stabilised the progressive failure caused by the CSC.

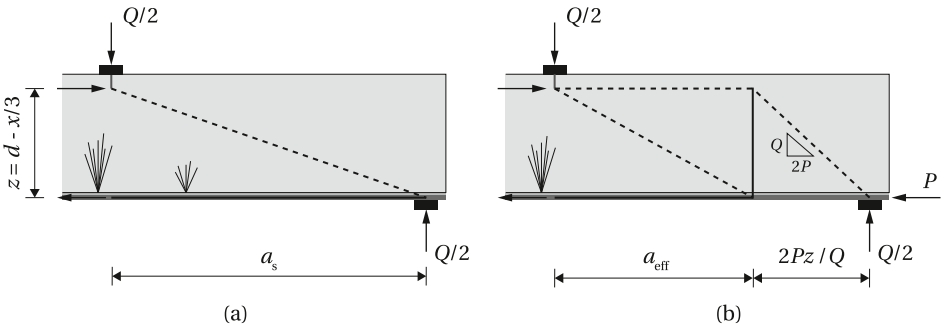

Fig. 4. Shear span of a reinforced glass beam (a) without and (b) with the application of post-tensioning; dashed line — compression, solid line — tension.

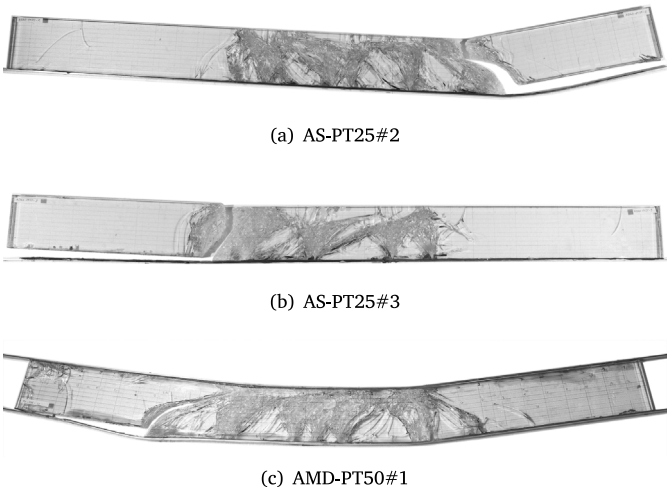

Fig. 5. Post-tensioned glass beam specimens after ultimate shear failure.

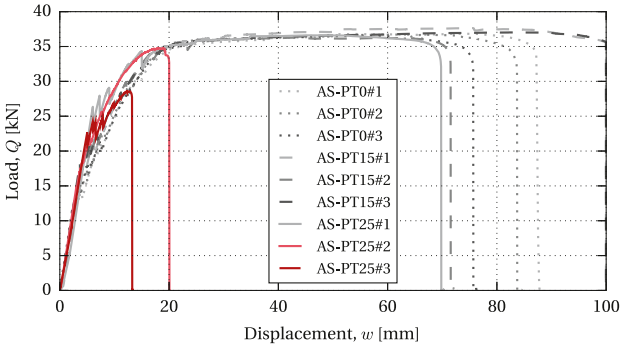

(a) Series AS

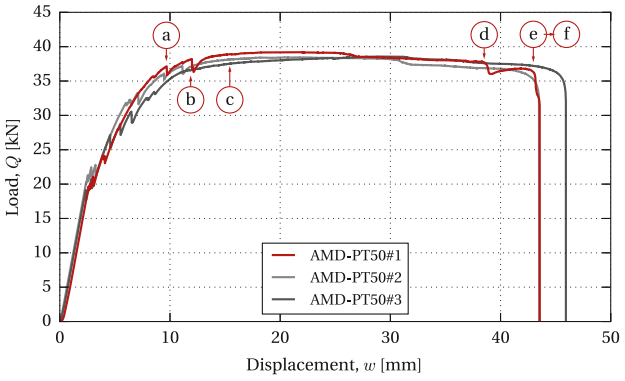

(b) Series AMD

Fig. 6. Load–displacement graphs of the complete series AS and AMS [7], with the specimens that developed a CSC highlighted in red. Stages of propagation of the CSC of the specimen AMD-PT50#1, shown in Fig. 7(a–f), are indicated with circular markers (a–f).

rotation formed at the crack tip, with normal and tangential relative displacements of the two beam parts separated by the CSC, clearly visible as the initial bond failure at the root of the crack (7(d)) started propagating towards the support (7(e)), finally leading to ultimate failure (7(f)). The stages of CSC propagation captured in Fig. 7 are indicatively marked on the load–displacement graph of the specimen AMD-PT50#1 in Fig. 6(b).

The kinematics of the critical shear crack of the specimen AMD-PT50#1 is schematically shown in Fig. 8, indicating the mechanisms potentially activated in shear transfer, resolved into vertical (Q) and horizontal components (N). The horizontal propagation of the crack diminishes the contribution of the cantilever action at an early stage. The total shear force Q_{tot} that can be transferred through the CSC can be considered as a sum of the vertical components of the remaining forces acting on the rigid body defined by the shape of the crack

$$Q_{tot} = Q_{res} + Q_{si} + Q_{cb} + Q_{dow} + Q_{ch} \quad (1)$$

where

- Q_{res} is the vertical component of the residual tensile strength of glass;
- Q_{si} is the vertical component of the surface interlock;
- Q_{cb} is the vertical component of the crack bridging by the interlayer;
- Q_{dow} is the dowelling action of the bottom tendon;
- Q_{ch} is the vertical component of the inclined compression chord.

The contribution of the residual tensile strength of glass is here neglected, given its low fracture toughness (K_{Ic} = 0.75 MPa m$^{0.5}$) [22]. Furthermore, the dowelling action is assumed to have little impact, since it fully depends on the stiffness of the adhesive, which is rather low compared to the stiffness of the glass beam and the steel tendon. Young's modulus of the applied adhesive ($E_a \approx 600$ MPa) is two–three orders of magnitude lower than the Young's modulus of glass (E_g = 70 GPa) and stainless steel (E_s = 180 GPa) [7]. This assumption is supported by the observed failure kinematics: the crack quickly propagates to ultimate failure in the final stage of the test, once the shear force is sustained only by the dowelling action. Therefore, the main contribution in shear transfer can be assigned to the surface interlock, crack bridging and inclined compression chord.

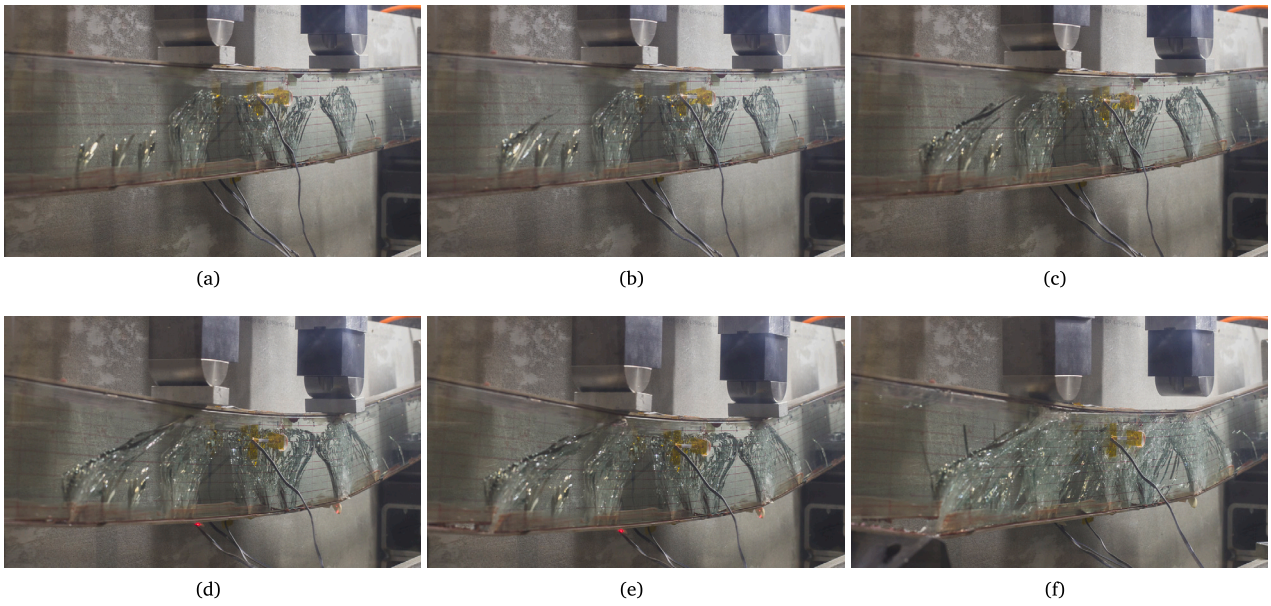

Fig. 7. Propagation of the critical shear crack of the specimen AMD-PT50#1.

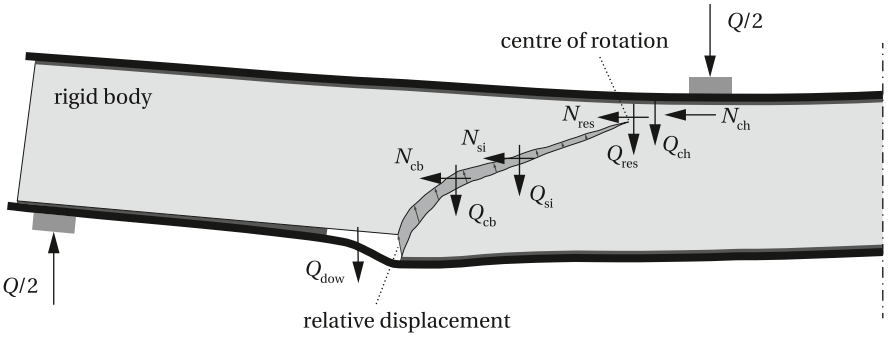

Fig. 8. Schematic of the critical shear crack kinematics and shear-transfer actions of the beam specimen AMD-PT50#1.

While this qualitative analysis provides a good basis for preliminary investigations of shear failure, further research is necessary in order to quantitatively estimate each shear-transfer action. Firstly, a refined measurement of the crack kinematics, i.e. relative opening and slip of the crack lips, should be performed during four-point bending tests, for instance, using digital image correlation technique for a 3D measurement of the displacement field on the beam surface [17]. Based on the readings of the displacement field (crack geometry and associated kinematics), the contribution of each potential shear-transfer action can be calculated by integrating the stresses along the CSC and ensuring the equilibrium conditions (vertical, horizontal and equilibrium of moments) [18]. The stress distribution associated with various shear-transfer mechanisms can be determined based on underlying fundamental constitutive laws of the materials. In case of post-fracture behaviour of reinforced and post-tensioned glass beams, these mechanisms are largely unexplored, most importantly the behaviour of fractured (SG) laminated glass under mixed-mode loading, which might explain the combined effect of surface interlock and crack-bridging. These mechanisms influence both flexural and shear capacity of reinforced and post-tensioned glass beams [7]. In Section 4, a novel testing methodology for simulation of stresses at the interface of CSC under mixed-mode loading is presented. A limited set of initial exploratory experiments aims to validate the feasibility of this method for derivation of constitutive laws for surface interlock and crack-bridging.

4. Exploratory double-notched mixed-mode tests

A limited set of double-notched mixed-mode tests (DNMMT) were carried out on pre-cracked SG-laminated glass specimens subjected to opening (tension) and sliding (shear) of the crack, with varying angle of the resultant of the applied displacement, i.e. opening angle ($\alpha = 0, 30, 45, 60°$). The aim of this exploratory study is to demonstrate the feasibility of a testing methodology, originally applied for the investigation of the mechanics of aggregate interlock in concrete [23], for the simulation of the stresses at the interface of a critical shear crack in glass laminates under mixed-mode loading. The specimens, based on the 25 mm thick laminated glass section applied in the post-tensioned beam tests (Fig. 1), were cut with a water jet into 120 mm wide and 110 mm high pieces, with 35 mm long notches to obtain a crack length $CL = 50$ mm (Fig. 9). The test area $CL \times B = 50$ mm $\times$ 25 mm, where B is the overall thickness of the specimen. A pre-damage, in form of a linear scratch along the front and back surfaces and the edges of a double-notched specimen, was applied by scoring the glass with a wheel cutter to predetermine the location of the crack, lower the initial fracture load and reduce crack-branching in the pre-cracking part of the test. It was generally applied in the centre of the notch, aligned over the three glass layers (with the exception of one specimen, shown in Fig. 9(c), which included an offset between the scratches due to lack of precision). An offset between the cracks in glass can be included as a parameter, simulating the non-alignment of glass cracks over multiple glass layers,

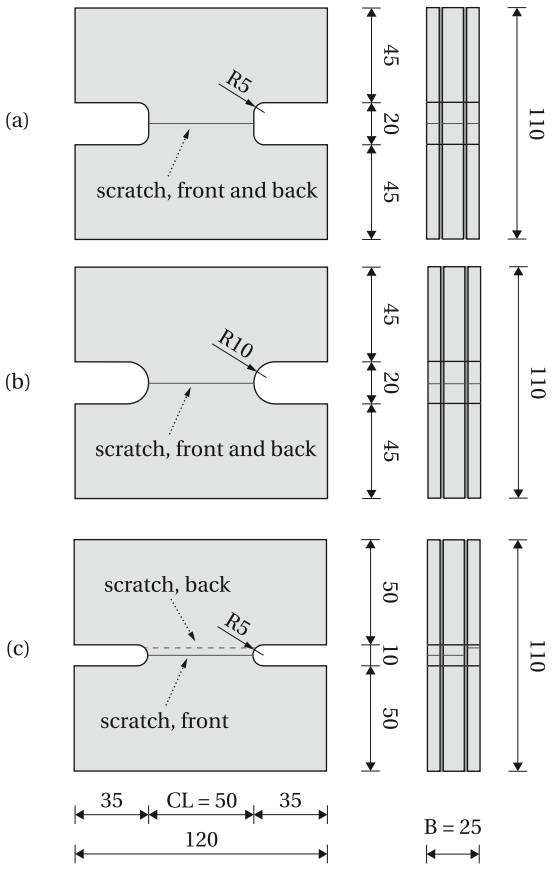

Fig. 9. Double-notched specimens for investigation of mixed-mode behaviour of fractured laminated glass: (a) Type A — wide straight notch; (b) Type B — wide round notch; (c) Type C — round notch; all dimensions are given in millimetres.

which is regularly observed in bending experiments. Specimens with a wide round or straight edge inside the notch allow for a larger spacing between the cracks (Fig. 9(a,b)).

A test setup developed by Tirassa et al. [23] was reused (Figs. 10 and 11) and mounted in a compression–tension machine Zwick 500 kN with an additional 50 kN hydraulic jack for the application of horizontal displacement. The intended test protocol, schematically shown in Fig. 10(c), consisted of, first, opening the cracks in mode I (tension) by applying a normal/vertical force F_N. Once a predefined initial crack opening was reached (w_{in} = 0.05 mm), the specimen was loaded in mixed mode (tension+shear), through the addition of the shear/horizontal force F_S. The relative opening and slip of the cracked specimen was monitored by means of bidirectional gauges (Fig. 11(b)), i.e. two strain gauges connected perpendicularly in order to simultaneously measure horizontal and vertical displacements. The tests were displacement controlled with initial speed of 1 μm/s, which was progressively increased as the measured force decreased from its peak value.

A total of eight specimens were tested, only few of which provided conclusive results in this preliminary phase. All the tests are listed in Table 1, indicating the type of notch, applied pre-damage, initial crack opening (w_{in}), opening angle (α), maximum normal force reached in the pre-cracking phase ($F_{N,max}$), and the maximum shear force reached in the mixed-mode phase ($F_{S,max}$). In this respect, it should be emphasized that the experiments were of exploratory nature.

The first specimen was tested without the pre-damage, which required a higher pre-cracking load ($F_{N,max}$) and resulted in a highly

Table 1
Double-notch mixed-mode tests (DNMMT) on pre-cracked SG-laminated glass specimens; notch type refers to Fig. 9.

No.	Type	Pre-damage	w_{in} [mm]	α	$F_{N,max}$ [kN]	$F_{S,max}$ [kN]
1	A	–	0.05	60°	14.57	1.98
2	A	aligned	0.05	30°	11.82	3.09
3[a]	B	aligned	0.05	45°	–	–
4	B	aligned	0.05	45°	9.02	1.04
5[a]	B	aligned	0.05	30°	–	–
6	B	aligned	0.05	30°	9.66	8.00[b]
7	B	aligned	0.05	0°	10.47	8.00[b]
8	C	offset	0.05	45°	7.54	1.86

[a]Invalid test; the specimen failed due to a setup error.
[b]Limit of the test setup.

branched initial crack. Specimens DNMMT#3 and #5 failed due to a setup error before the initial pre-cracking was achieved. In the remaining tests, the fracture was generally initiated from the scratched edge surface inside the notch, which propagated into a relatively straight crack throughout the specimen. The pre-cracking did not occur concurrently in all three glass layers. Given that problems with the bidirectional gauges were observed in certain tests (detachment of one of the gauges, interrupted or reset signal), rendering the collected displacement data unreliable, only two exemplary test results of *Type B* specimens (Fig. 9(b)) — DNMMT#4 and #7 — tested at 45° and 0°, respectively, with aligned pre-damage of the three glass layers, are further analysed in detail. Figs. 12 and 13 show the development of normal stresses vs. vertical displacement and shear stresses vs. horizontal displacement, as well as images of the specimens before and after the test. The average normal stress in the area between the notches is defined as $\sigma = F_N/(CL \cdot B)$. Similarly, the average shear stress equals $\tau = F_S/(CL \cdot B)$. The stress peaks in the normal stress–displacement diagrams correspond with the initial pre-cracking of the glass layers. After the pre-cracking, the specimen DNMMT#7 shown in Fig. 12 was subjected to horizontal displacement (α = 0°), reaching the force limit of the test setup (8 kN) with a resulting shear stress of 7.27 MPa (Fig. 12(a)). The vertical force switched from tension in pre-cracking to compression in mixed mode in order to maintain the initial crack opening of 0.05 mm. With the increase in horizontal displacement/shear stress, secondary inclined cracks developed along the initial crack due to the effect of the surface interlock (Fig. 12(b)). The specimen DNMMT#4 in Fig. 13 was subjected to equivalent vertical and horizontal displacement following the pre-cracking (α = 45°). With the addition of crack opening, a shear stress of only 0.95 MPa was reached (Fig. 13(a)). The cracks concentrated along the straight initial fracture (Fig. 13(b)). The test was stopped due to the horizontal displacement limit of the setup (~2.2 mm) after reaching the peak shear stress. No delamination could be observed in any of the tested specimens.

Although limited in the number of specimens, this preliminary study has demonstrated the feasibility of the applied test methodology for the investigation of mechanical parameters that influence the combined shear transfer mechanism of surface interlock and crack bridging. By simulating the opening and the sliding of the CSC on small-scale specimens, a more detailed analysis of the stresses that develop along the crack surface (combined with the stresses within the interlayer bridging the cracks in the glass) can be performed. The presented exemplary test results show that DNMMT can simulate the response of a fractured laminated glass section under varying opening angles. In order to provide a more conclusive law that relates the maximum shear and tensile stresses with the angle of the resultant of the applied displacement (α), a larger systematically designed experimental study should be conducted, taking into account different levels of the initial crack opening. This should enhance the understanding of mixed-mode load transfer in fractured laminated glass and provide the basis for the determination of a constitutive model describing the shear stress–slip relationship along the crack lips.

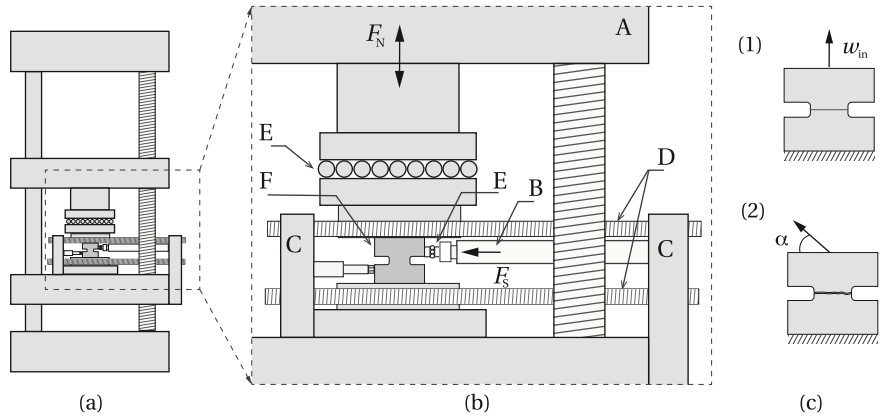

Fig. 10. Schematic of the DNMMT setup, adapted from [23]; (a) general and (b) detailed view: A — compression–tension machine, B — horizontal jack, C — reaction plates, D — threaded bars, E — sliding rails, F — test specimen; (c) test kinematics: (1) initial crack opening up to $w_{in} = 0.05$ mm; (2) mixed-mode loading, with an opening angle α.

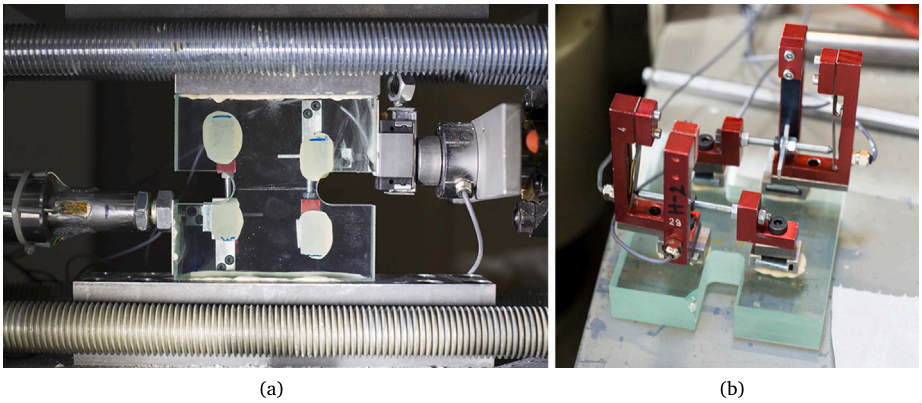

Fig. 11. Double-notched glass specimen in the mixed-mode test setup (a), with bidirectional gauges (b).

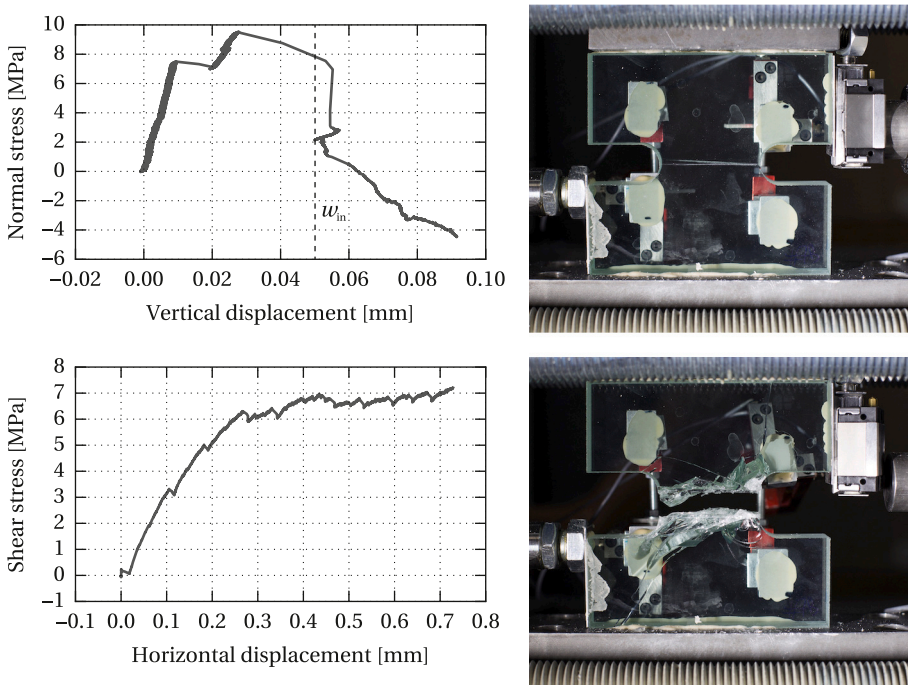

Fig. 12. Double-notched mixed-mode test #7 at $\alpha = 0°$; (a) normal and shear stress–displacement plots; (b) specimen before (top) and after the test (bottom).

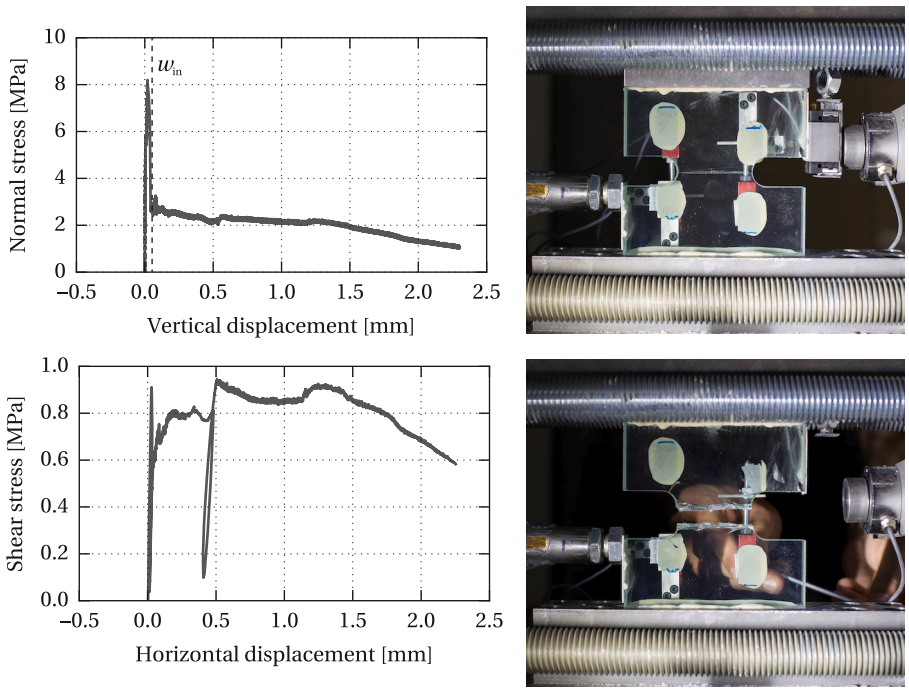

Fig. 13. Double-notched mixed-mode test #4 at $\alpha = 45°$; (a) normal and shear stress–displacement plots; (b) specimen before (top) and after the test (bottom).

5. Discussion

The process of shear failure observed in the study of flexural behaviour of post-tensioned glass beams was characterised by sudden nature of ultimate failure due to the development of a critical shear crack, which places those beams on the right side of the Kani's valley, $a_s/d > \gamma_2$, or further on the right plateau, $a_s/d > \gamma_3$, in case of the specimen AMD-PT50#1, which reached full flexural capacity. The shear slenderness of the tested beam specimens equals 4 (a_s/d = 500 mm/125 mm). In order to assess the values γ_1, γ_2 and γ_3 that define the region of reduced beam strength for reinforced and post-tensioned glass beams, a range of specimens with varying shear slenderness should be further investigated.

The level of post-tensioning should be varied within the yielding limit of the applied reinforcement to clarify its influence on the shear strength of glass beams. In the experimental study reported in [7], pre-load applied on the tendons was varied in three steps in the series AS (Fig. 1(a)) — 0, 15 and 25 kN. While both series with a 0 and 15 kN pre-load reached full flexural capacity, increasing the pre-load to 25 kN resulted in 2/3 beams failing in shear (Fig. 6(a)). Although the application of post-tensioning is expected to enhance the shear resistance by limiting the opening of the cracks (Fig. 4), the addition of an increased level of post-tensioning and bending induced strains in the tendon prematurely reached the plastic plateau, resulting in increased rotations and opening of the CSC, thus limiting the shear capacity of the two beams.

The kinematics of shear failure depends on the location and shape of primary flexural cracks and their progression during the process of loading (relative to the position of the direct compression strut carrying shear from the load point to the support point). Given that the fracture of glass beams in bending initiates from critical flaws randomly distributed on the surface subjected to tensile stresses, the location of cracks may vary considerably. Hence, a significant number of specimens need to be tested in order to systematically analyse CSC kinematics. Refined measurements of the displacement field are necessary for a detailed analysis of the crack evolution and the transfer of forces between various potential shear-transfer actions by establishing rigid-body diagrams, as demonstrated in this preliminary study (Fig. 8). A database of typical shear failure kinematics, which takes into account a large number of specimens with different geometrical and mechanical properties, and the development of suitable constitutive laws of the applied materials will provide a basis for design recommendations for the prediction of shear resistance of reinforced and post-tensioned glass beams.

6. Conclusions

The qualitative analysis of the kinematics of shear failure, presented in this paper, may serve as a basis for future investigations of shear resistance of glass beams. Specific shear transfer actions which govern the shear failure kinematics of reinforced and post-tensioned beams have been identified, as well as the main parameters which influence the shear capacity, such as the beam slenderness and level of post-tensioning. Further research is necessary to quantitatively estimate each shear-transfer action, which, summed up, correspond with the shear capacity of the beam. A refined measurement of the crack kinematics, i.e. relative opening and slip of the crack lips, is necessary for a detailed analysis of the contribution of various potential shear-transfer actions. Additionally, for the prediction of the shear (and flexural) capacity of glass beams in the post-fracture state, a better understanding of the mixed-mode behaviour of fractured (SG) laminated glass is essential. Preliminary experiments on small-scale double-notched specimens have demonstrated the feasibility of the applied test methodology for the simulation of the stresses at the interface of a critical shear crack under mixed-mode loading. Further investigations are necessary to determine a constitutive model describing the shear stress–slip relationship along the crack lips.

Preliminary research has shown that shear failure may significantly reduce the flexural capacity of reinforced glass beams in the post-fracture state. Better understanding of the risk of shear failure will therefore contribute to the safety of glass applications in construction. A detailed study of shear failure kinematics on a significant number of specimens is essential for providing design recommendations for the prediction of shear resistance of reinforced and post-tensioned beams, together with the development of suitable constitutive laws of the applied materials.

CRediT authorship contribution statement

Jagoda Cupać: Conceptualization, Methodology, Investigation, Writing – original draft, Writing – review & editing, Visualization, Funding acquisition. **Christian Louter:** Writing – review & editing, Supervision, Funding acquisition. **Alain Nussbaumer:** Conceptualization, Methodology, Writing – review & editing, Supervision, Funding acquisition.

Declaration of competing interest

The authors declare that they have no known competing financial interests or personal relationships that could have appeared to influence the work reported in this paper.

Data availability

Data will be made available on request.

Acknowledgements

The authors would like to thank the Swiss National Science Foundation for funding the present research through SNSF Grants 143267 and 159914, Dr Miguel Fernández Ruiz for taking an interest in glass and sharing his expertise on critical shear crack theory, and Max Tirassa for lending his time and infrastructure allowing us to perform the preliminary mixed-mode tests.

References

[1] Feldmann M, Di Biase P. The CEN-TS "Structural glass - design and construction rules" as pre-standard for the eurocode. ce/Papers 2018;2(5–6):71–80. http://dx.doi.org/10.1002/cepa.911.

[2] Martens K, Caspeele R, Belis J. Development of reinforced and posttensioned glass beams: Review of experimental research. J Struct Eng 2016;142(5):04015173. http://dx.doi.org/10.1061/(ASCE)ST.1943-541X.0001453.

[3] Bos F, Veer F, Hobbelman G, Louter C. Stainless steel reinforced and post-tensioned glass beams. In: ICEM12 - 12th international conference on experimental mechanics. Bari; 2004.

[4] Louter C, Cupać J, Lebet J-P. Exploratory experimental investigation on post-tensioned structural glass beams. J. Facade Des. Eng. 2014;2(1–2):3–18. http://dx.doi.org/10.3233/FDE-130012.

[5] Jordão S, Pinho M, Martin JP, Santiago A, Neves LC. Behaviour of laminated glass beams reinforced with pre-stressed cables. Steel Constr 2014;7(3):204–7. http://dx.doi.org/10.1002/stco.201410027.

[6] Engelmann M, Weller B. Residual load-bearing capacity of spannglass-beams: effect of post-tensioned reinforcement. Glass Struct Eng 2019;4(1):83–97. http://dx.doi.org/10.1007/s40940-018-0079-4.

[7] Cupać J, Louter C, Nussbaumer A. Flexural behaviour of post-tensioned glass beams: Experimental and analytical study of three beam typologies. Compos Struct 2021;255:112971. http://dx.doi.org/10.1016/j.compstruct.2020.112971.

[8] Bedon C, Louter C. Structural glass beams with embedded GFRP, CFRP or steel reinforcement rods: Comparative experimental, analytical and numerical investigations. J Build Eng 2019;22:227–41. http://dx.doi.org/10.1016/j.jobe.2018.12.008.

[9] Silvestru V-A, Deng Z, Michels J, Li L, Ghafoori E, Taras A. Application of an iron-based shape memory alloy for post-tensioning glass elements. Glass Struct Eng 2022;7:187–210. http://dx.doi.org/10.1007/s40940-022-00183-z.

[10] Ølgaard AB, Nielsen JH, Olesen JF. Design of mechanically reinforced glass beams: modelling and experiments. Struct Eng Int 2009;19(2):130–6. http://dx.doi.org/10.2749/101686609788220169.

[11] Louter C, Belis J, Veer F, Lebet J-P. Structural response of SG-laminated reinforced glass beams; experimental investigations on the effects of glass type, reinforcement percentage and beam size. Eng Struct 2012;36:292–301. http://dx.doi.org/10.1016/j.engstruct.2011.12.016.

[12] Agnetti S, Speranzini E. Hybrid steel-fibre reinforced glass beams – experimental and numerical analysis. In: Challenging glass 4 & COST action TU0905 final conference. Lausanne; 2014, p. 211–8.

[13] Firmo F, Jordão S, Neves LC, Bedon C. Exploratory study on simple hybrid or pre-stressed steel-glass I-beams under short-term bending - Part 1: Experiments. Compos Struct 2020;234:111651. http://dx.doi.org/10.1016/j.compstruct.2019.111651.

[14] Wang ZY, Shi Y, Wang QY, Wu Y, He M. In-plane shear compression behaviour of steel-glass composite beams with laminated glass webs. Eng Struct 2017;150:892–904. http://dx.doi.org/10.1016/j.engstruct.2017.07.076.

[15] Campione G, Cannella F, Cavaleri L. Flexural behavior of hybrid glass beams with rectangular cross-sections. Constr Build Mater 2018;181:134–45. http://dx.doi.org/10.1016/j.conbuildmat.2018.06.017.

[16] Zhang D, Chen S, Lu Y, Chen X. Quasi-static experimental study on flexural performance of aluminum-reinforced laminated glass beams. Eng Struct 2022;256:113993. http://dx.doi.org/10.1016/j.engstruct.2022.113993.

[17] Cavagnis F, Fernández Ruiz M, Muttoni A. An analysis of the shear-transfer actions in reinforced concrete members without transverse reinforcement based on refined experimental measurements. Struct Concrete 2018;19(1):49–64. http://dx.doi.org/10.1002/suco.201700145.

[18] Muttoni A, Fernández Ruiz M. From experimental evidence to mechanical modeling and design expressions: The critical shear crack theory for shear design. Struct Concrete 2019;20(4):1464–80. http://dx.doi.org/10.1002/suco.201900193.

[19] Vaz Rodrigues R, Fernández Ruiz M, Muttoni A. Influence of shear on rotation capacity of reinforced concrete members without shear reinforcement. ACI Struct J 2010;107(3):516–25. http://dx.doi.org/10.14359/51663902.

[20] Fernández Ruiz M, Muttoni A, Sagaseta J. Shear strength of concrete members without transverse reinforcement: A mechanical approach to consistently account for size and strain effects. Eng Struct 2015;99:360–72. http://dx.doi.org/10.1016/j.engstruct.2015.05.007.

[21] Campana S. Eléments en béton armé soumis à une combinaison de flexion, effort tranchant et forces de déviation (Ph.D. thesis), 5574, EPFL; 2013.

[22] Haldimann M, Luible A, Overend M. Structural use of glass. Zürich: IABSE; 2008, p. 57.

[23] Tirassa M, Ruiz MF, Muttoni A. Modern experimental research techniques for a consistent understanding of aggregate interlocking. In: Proceedings of the 12th Fib PhD symposium in civil engineering. Prague; 2018.